Forecasting of Photovoltaic Power with ARO based AI approach

Srinivasa Rao Bittla
Independent Researcher
sbittla@gmail.com

Srimaan Yarram
Independent Researcher
srimaan.yarram@gmail.com

Abstract—Sunlight is the key to renewable power that can supply the smart grid of the future with vast quantities of electricity. Unfortunately, the unpredictability and intermittent nature of solar energy resources provide challenges for the systems. Future smart grid optimization and planning are significantly hampered by solar power's inherent unpredictability. Reducing the intermittent nature of power requires a precise estimation of photovoltaic (PV) power generation. Predicting PV power with high accuracy is critical for reducing the potential for grid disruptions caused by the addition of PV plants.Hence, we present a Network (CNN) architecture for short-term power forecasting based on transfer learning and AlexNet. The input is chosen based on past power, sun radiation, wind speed, and temperature readings. The artificial rabbit technique is used to pick the best possible values for AlexNet's hyper-parameters (ARO). The tracking efficiency of existing local solutions is then increased by incorporating the selective opposition method into ARO. All input parameters are transformed to 2D feature maps and fed into the CNN's input in order to features. After a thorough evaluation on real PV data from Limberg, Belgium, the numerical findings show that the presentation in PV schemes.

Keywords— Convolutional Neural Network; Artificial rabbit algorithm; Power systems; Lévy flight; AlexNet.)

I. INTRODUCTION

Research into the safety, availability, and long-term viability of energy sources has grown in prominence in recent years. The world over, people are interested in finding answers to issues caused by the limitations of conventional energy. It is common knowledge that conventional energy sources are harmful to the ecosystem and cannot be used indefinitely. Using renewable energy sources is one solution to these issues, according to the studies conducted on the topic [2-3]. Solar power systems are an important alternative energy option. availability, solar energy has the potential to be a more acceptable and attractive energy source. It has numerous benefits, including zero environmental impact, unlimited accessibility, and no cost to use. Thermal (PV) solar power generation are the two main categories [4]. Among them, PV is seen as one of the most promising power generation technology due to its potential to offer clean and. (PV) systems utilise PV cells to generate electricity from sunlight [5]. As the price of PV systems continues to drop, they become more practical for use in both residential and commercial settings, lowering the overall cost of power generation. This is why photovoltaic power plants (PVPPs) have expanded fast in both size and number as a primary source of electricity generation around the world [6].

Researchers all across the world have recently shown a lot of interest in PV power generating. Physical approaches, statistical methods, and AI methods are the three main types of PV prediction techniques [7]. Numerical weather prediction (WWP), sensing measurement, and ground measurement devices are all used in the physical technique to collect meteorological and geological information. Nonetheless, maintenance facilities must undergo proper and periodic calibration [8]. The strategy for predicting PV's future behaviour via error minimization by extracting features from training samples. Reliable predictions of PV production power rely on the quality of available historical samples [9]. Meanwhile, AI methods have matured into a valuable resource for both wind and PV generation [10, 11] and offer a solution to the challenge of non-linear function estimate [12]. To automatically parametrize the Voltage- PV modules [13], for instance, neural networks can be employed to simulate the characteristics of conventional silicon-based PV modules. At the same time, AI is playing an increasingly important role in the energy sector, particularly in areas like the control system, energy recognition, and failure categorization [14, 15]. Specifically, it is better to previous replicas in dealing with non-linear glitches with large uncertainty [16], thanks to the rapid development of procedures and great performance in various sectors.

Deep neural networks like CNNs have several hidden layers before the output. The recent advancements in hardware systems have methods, and CNNs have attained state-of-the-art solutions in many high-level issues. CNNs allow us to learn more nonconcrete and efficient features in PV power forecasting issues than shallow learning does. Nevertheless, the aforementioned techniques ignore important weather changes in the PV data since they don't include the context of preceding days. Next, we investigate whether the forecasting model's performance improves if we incorporate the past information of the days that came before the current one. With the preceding considerations in mind, this study proposes a deep convolutional neural network (CNN) architecture based power forecasting system for a grid-tied PVPP that can withstand extreme weather. Predicting PV power one to five hours in advance using the AlexNet architecture. Radiation, temperature, wind speed, and electrical power records from the past are used as input factors. In this way, the convolution blocks are able to extract any deep characteristics that are inherent to the data. The ARO model, which will be labeled in detail in the following section, is responsible for adjusting AlexNet's hyper-parameters.

Below is a rundown of the rest of the paper: The relevant literature is presented in Part 2, and the suggested model is explained in depth in Section 3. In Section 4 we provide the results of our experimental investigation. Part 5 provides a summary and conclusion of the study..

II. . RELATED WORKS

First, the data is pre-processed with ensemble empirical mode decomposition and modal identification is achieved with stationarity analysis; second, forecasts are generated using a combination of support vector regression optimised with the sparrow search algorithm and statistical methods, Third, experimental testing is conducted to determine the method's efficacy in the context of renewable energy time series prediction. The experimental results show that the proposed model improves the accuracy and prediction performance of ultra-short-term renewable energy forecasting, and that it is both broadly applicable and competitive across a variety of forecasting scenarios and characteristics.

hyperfine optimal dispatch approach for IEM that accounts for uncertainty. The suggested method not only prediction error based on distributionally robust optimization, but also shows how time resolution affects the best dispatch of integrated energy (DRO). A piecewise McCormick algorithm with parallel processing is built to deal with the given model's

complexity and non-convexity. The case studies are carried out to show how the suggested optimal dispatch is advantageous in computation time, and resilience.

In order to mitigate the negative effects of solar photovoltaic (PV) systems on the natural world .The proposed method is called the SSA-GBDT methodology since it combines the sparrow search procedure and the gradient boosting decision tree. The method suggested here aims to maximise the power extracted from PV arrays and increase the complete efficiency of solar PV energy systems. SSA measures the voltage, current, and power of the PV modules in an offline setting. The GBDT online model development process makes use of a database including electric parameters. Particle size, dust weight, and the maximum power value are only a few of the input and output characteristics represented in the data set. Once the projected method has been developed, it is implemented on the MATLAB/Simulink platform and its performance is compared to that of other methods. The effectiveness of PV is examined under a variety of scenarios, including regular operation, dust collection, water drops, and partial shadowing. Cases are analysed using active and reactive power, grid current and voltage, and inverter power in addition to the standard photovoltaic (PV) input and output conditions of irradiance and temperature. PV power efficiency comparisons for several solution techniques are also analysed, including ANN, GBDT, SSA, and the suggested system.

We were able to compare and analyse the best irrigation strategy by using this flexible tool to generate irrigation schedules for combinations of subunits studied individually (with a standard deviation in the applied water sheet of 2.8 m3ha1) and for combinations of several subunits studied working together. Using a high-power solar pumping system in Albacete, Spain, the I-Selector model has developed irrigation plans to determine the optimum sequence of opening combinations of subunits distributed over time slots each day.

III. PROPOSED SYSTEM

In this proposed methodology, Predicting PV power with high accuracy is critical for reducing the potential for grid disruptions caused by the addition of PV plants. Hence, we present a Network (CNN) architecture for short-term power forecasting based on transfer learning and AlexNet. The input is chosen based on past power, sun radiation, wind speed, and temperature readings. The artificial rabbit technique is used to pick the best possible values for AlexNet's hyper-parameters (ARO). The tracking efficiency of existing local solutions is then increased by incorporating the selective opposition method into ARO. All input parameters are transformed to 2D feature maps and fed into the CNN's input in order to features

A. The PV power data

We take into account a dataset of PV power generation over the course of a year, with daily data spanning 5:00 to 19:00 UTC at a resolution of 15 minutes. If we define D as the number of days in the PV data period and M as the points each day, we get the following. Let the mth power point of the dth day, denoted by p dmR, for m in [1,...,M] and d in [1,...,D]. An output power matrix can be obtained by multiplying fpm by d and gd by m. $\tilde{P} \in R^{D\times M}$, ie.,

$$\tilde{P} = \begin{bmatrix} p_1^1 & \cdots & p_1^M \\ \vdots & \cdots & \vdots \\ p_D^1 & \cdots & p_D^M \end{bmatrix} (1)$$

We'll refer to p d as = [p d1,..., p dM]. dth-day output power of TRM as the symbol. p m = [p 1m,...,p Dm]. The mth output power point on different days is represented by the mth column vector of P, denoted by TRD. This article details the energy generated by photovoltaic panels in Flanders between July 1st and the 10th.

There is some regularity to the way the PV power sequence shifts over successive days. The seventh and eighth sequences, for example, share a similar output power on consecutive days,

suggesting that these days also share a similar climate. The output power of the eighth, ninth, and tenth sequences has augmented dramatically over time, and perhaps the weather situation on the tenth day is more conducive to the development of PV plants. Hence, the output power sequences of consecutive days can reveal a general tendency in the weather. Due to the unpredictability of the weather, the output power of the second day may vary significantly from the first, as evidenced by the fifth, sixth, and seventh sequences. While daily averages are useful, the output power sequences of neighbouring days can provide more meteorological information for power predictions.

Clearly, there is a high degree of ambiguity regarding the output power points on various days, and the sequence is unstable. It seems to reason that the weather is the primary factor in determining the amount of solar energy available. Red dashed lines show a roughly linear relationship between output power and time. It is evident at the same time on prior days can be utilised to forecast the PV power on the next day. As an added bonus, an AI-based technique is used to discover an input-output mapping..

B. . Correlation between the adjacent days

We consider a year (D=360 days) to investigate the relationship between the power output at different times. Daily data are collected between 5:00 and 19:00 UTC (M=60), with a resolution of 15 minutes. On day I the output power is given by p i=[p i1,...,p iM]T,i[1,...,D]. After that, we use the cosine similarity [25] and correlation coefficient [26] to compare the PV output power on consecutive days. Here is how we define the metrics:

$$c_{ij} = \frac{\sum_{m=1}^{M} p_i^m p_j^m}{\sqrt{\sum_{m=1}^{M}(p_i^m)^2}\sqrt{\sum_{m=1}^{M}\left(p_j^m\right)^2}} \quad (2)$$

$$r_{ij} = \frac{\sum_{m=1}^{M}(p_i^m - p_i^{avg})(p_j^m - p_j^{avg})}{\sqrt{\sum_{m=1}^{M}(p_i^m - p_i^{avg})^2\left(p_j^m - p_j^{avg}\right)^2}} \quad (3)$$

$$C_k = \frac{1}{D-k}\sum_{i=1,j=i+k}^{D-k} c_{ij}\,, R_k = \frac{1}{D-k}\sum_{i=1,j=1+k}^{D-k} r_{ij} \quad (4)$$

Specifically, for any given day j in the range [1,...,D], the output power at the mth power point on day j is denoted by pm j, and p j=[p j1,...,p jM]. ^ The value T.k represents the time span between the ith and jth days (i+k=j). The average values for today, the ith day, and yesterday, the jth day, are denoted by p I avg and p j avg, respectively. Cosine similarity (c ij) and correlation coefficient (r ij) between the ith and jth days. This average cosine similarity value is denoted by the symbol C k. As with R k, the average value of the correlation coefficient is represented by R k. Using k=[1; ; K] and K=60, we determine C k and R k. The picture also displays the outcome of a polynomial regression. Both measures drop as k grows, as evidenced by the graphs. When k is significant, it's reasonable to assume that the weather will be very different from the average. A high cosine similarity and correlation coefficient between two days indicates that the weather between them might not fluctuate much, especially when k is small. This suggests that looking at PV data from the days surrounding the current one can help more accurately predict output power. As a result, the PV data from the days prior is used to enhance the prediction performance of PV systems..

C. . Prediction of PV using AlexNet architecture

The developed network's ability to learn deep characteristics and predict nonlinear outputs in the forecasting problem is the driving force behind the design. In order to fully exploit image recognition and extract high-level features with varying degrees of visual perception, a straightforward and effective CNN model is built with AlexNet. If you're having trouble with picture identification, AlexNet is a CNN architecture that performs exceptionally well. Five convolution layers, three max-pooling levels, three fully connected layers, and one regression layer make up the AlexNet's total of 12 layers.

Convolution layers in the network use filters with kernel sizes of 11 by 11, 5 by 5, and 3 by 3. Filters in max-pooling layers are just 3x3. Extraction of high-level feature maps is made possible by computing the neuron output with the help of these compact filters. In the initial convolution, we use a stride level of 4 to minimise the dimensions of the feature maps. All the rest are assigned the value 1. Following the initial two convolutions, noise is suppressed via Cross Channel Normalization (CCN) layers. The output of the ith layer, fy i, is given as where m is the filter size of the ith layer (n), b is the bias matrix, and j determines the kernel.:

$f\{y_i^n\} = b_i^n + \sum_{k=1}^{m_i^{n-1}} j_{(i,k)}^n \times y_k^{(n-1)}$ (5)

With the use of ReLu functions, the convolutions are engaged to break down the noises. As a result, the ReLu function f's output can be written as:

$f(t) = \begin{cases} t & t \geq 0 \\ 0 & t < 0 \end{cases}$ (6)

Using a nearby outputs statistic, the max-pooling layer can be used to lower the dimensionality of the ReLu outputs, and its formula is as follows.;

$m_i = \max(F_R)\,|_{F=f_i} i \in R$ (7)

A new fully connected layer is attached to the fc-7, replacing the existing fc-8, softmax, and classification layers from the original AlexNet architecture. In this way, we can get a vector containing deep features. The input is multiplied by the weight matrix in the fully-connected layer, and the product is then added to the bias vector in Equation (9).:

$y_i^n = b_i^n + \sum_{k=1}^{m_i^{n-1}} w_{(i,k)}^n \times y_i^{(n-1)}$ (8)

Time-series power predictions are made using an image-independent regression layer as the final stage of the network. It's also worth noting that the challenging ImageNet supplies a well-trained AlexNet architecture, and that the network parameters from this pre-trained network can be used effectively to produce a brand new deep forecasting framework..

1) Optimization method

In order to extract the backpropagation phase, the proposed network's entire cost function is optimised utilising the SGD algorithm. Each iteration of the SGD optimization method aims to get closer to the target by adjusting the weights. The rule for updates can be stated as:

$\Lambda_{t+1} = \Lambda_t - \eta_t \;\; F(\Lambda_t, B_t)$ (9)

the cost function F(t,B t) is the mini-batch B t, and _t>0 is the learning rate. Inverse Hessian of G can be approximation using B t. The ARO model, which is described below, is used to pick the hyper-parameters optimally.:

2) . Artificial Rabbits Optimization (ARO)

The ARO algorithm is based mostly on two principles of rabbit survival in the wild: detour foraging and random concealment [27]. One such tactic is called "detour foraging," and it involves rabbits eating grass around their nests to avoid being spotted by predators. In order to conceal themselves even more thoroughly, rabbits will occasionally hop to nearby burrows. The initialization procedure is crucial to the launch of any search algorithm. It is assumed here that d is the dimension of the design variable, N is the number of rabbits in the simulated colony, and ub and lb are the upper and lower bounds, respectively. Next we perform the initialization in the ways described below..

$\vec{z}_{i,k} = r.(ub_k - lb_k) + lb_k, k = 1,2,\dots,d$ (10)

where z (i,k) represents the i-th rabbit's position in the j-th dimension, and r is a random value. Although both exploration and exploitation are taken into account by the metaheuristic algorithm, detour foraging focuses primarily on the former. Each rabbit may often leave the immediate area of the food supply to investigate a different rabbit's territory in the group. Below is the most recent formul for "detour foraging."

.

$$\vec{v}_i(t+1) = \vec{z}_j(t) + R.\left(\vec{z}_i(t) - \vec{z}_j(t)\right) + round\left(0.5.(0.05 + r_1)\right).n_1$$ (11)

$$R = l.C$$ (12)

$$l = \left(e - e^{\left(\frac{t-1}{T_{max}}\right)^2}.\sin(2\pi r_2)\right)$$ (13)

$$C(k) = \begin{cases} 1 & if\ \ k == G(l) \\ 0 & else \end{cases}\ lk = 1, \dots, d\ and\ l = 1, \dots, [r_3.d]$$ (14)

$$G = randp(d)$$ (15)

$$n_1 \sim N(0,1)$$ (16)

where v _(i,k) (t+1) indicates the artificial rabbit's new location, i,j = 1,...,N; z I represents the location of the ith artificial rabbit; and z _j signifies artificial rabbits located at other random points. The maximum number of cycles, denoted by T max, is undefined. The sign [] represents the ceiling function, which rounds to the nearest integer, while the symbol randp indicates a random permutation of the numbers from 1 to d. Random numbers r 1, r 2, and r 3 range from 0 to 1. The length L denotes the tempo at which one runs while foraging along a circuitous route. The value of n1 follows the expected normal distribution. N 1, a random number drawn from a normal distribution, best captures the nature of the disturbance. The last term in Equation (11) can be perturbed to aid ARO in avoiding local extremum and conducting a global search.

The exploration phase of the algorithm serves as inspiration for the random hiding phase, as rabbits will often create multiple tunnels near their nests and then pick one at random to hide in. For starters, we establish how rabbits create burrows at will. When the ith rabbit digs the jth hole, it is called a:

$$\vec{b}_{i,j}(t) = \vec{z}_i(t) + H.g.\vec{z}_i(t)$$ (17)

$$H = \frac{T_{max}-t+1}{T_{max}}.n_2$$ (18)

$$n_2 \sim N(0,1)$$ (19)

$$g(k) = \begin{cases} 1 & if\ \ k == k \\ 0 & else \end{cases}\ l\ k = 1, .., d$$ (20)

where i=1,...,N and j=1,...,d and n2 is normally distributed. With random fluctuations, the value of the hidden parameter H goes from 1 to 1/Tmax linearly. Figure 1 displays the 1000-iteration change in an's value. There is a smooth progression from exploration to exploitation depicted by a decreasing H value trend in the picture.

The inform formula for the random hiding technique is exposed below.

$$\vec{v}_i(t+1) = \vec{z}_i(t) + R.(r_4.\vec{b}_{i,r}(t) - \vec{z}_i(t))$$ (21)

$$g_r(k) = \begin{cases} 1 & if\ k == [r_5.d] \\ 0 & else \end{cases}\ l\ k = 1, \dots, d$$ (22)

$$\vec{b}_{i,r}(t) = \vec{z}_i(t) + H.g_r.\vec{z}_i(t)$$ (23)

Where v I (t+1) is the artificial rabbit's new position, i,r(t) is a burrow chosen at random from the d burrows made by the rabbit are random numbers we provide in the interval [0,1]. R is calculated using Eqs. (12)-(15). (15).

We then reset the position of the ith synthetic rabbit using Equation once the two update procedures have been put into effect (24).

$$\vec{z}_i(t+1) = \begin{cases} \vec{z}_i(t) & if\ \ f(\vec{z}_i(t)) \le f(\vec{v}_i(t+1)) \\ \vec{v}_i(t+1) & else\ f(\vec{z}_i(t)) > f(\vec{v}_i(t+1)) \end{cases}$$ (24)

We can think of this equation as an adaptive upgrade. Based on the adaption value, the rabbit will decide on its own whether to remain in its current location or search for a new one.

For optimization algorithms, populations favour carrying out the examination phase early on and the exploitation phase later. In order to perfect the shift from ARO uses the rabbits'

diminishing energy as a design metric for its discovery algorithm. Under the context of the algorithm of the synthetic rabbit, we define the energy component as:

$A(t) = 4.\left(1 - \frac{t}{T_{max}}\right).In\frac{1}{r}$ (25)

If r is some random number and r is what happens when (0, 1). The variation of during a period of 1000 iterations with respect to. By analysing the data presented in the image, we see that the value of A is falling, which ensures a smooth transition from exploration to exploitation as the iterations progress.

IV. Results and Discussion

Here we provide the results of our trials and analyses of the proposed deep prediction system. The evaluation metrics of the projected method are associated and contrasted with the most popular regression algorithms, and their effects are addressed. The experiments are run in a MATLAB environment, with an Intel (R) i7-10750 H CPU running at 2.60 GHz, an NVIDIA Quadro P620 GPU, and 16 GB RAM..

4.1. Dataset Description

Elia, the Belgian electricity transmission system operator, provided the freely downloadable and accessible historical PV output power data used in the simulation [28]. Using data from the Limberg PV power facility, a prediction model is developed and put through its paces. Keep in mind that the active power of the PV plants is measured in real time with the help of an active power flow metre, and that its measurement error is less than 0.5%. Power is discussed in terms of measured power, as the measurement error is typically negligible and the measured power is considered to be the PV plants for the purposes of this article. So, the measurement mistakes are ignored in the experiments, as is the case with other PV power forecast publications.

The PV power plant has a 451.82 MW rated capacity and a 0 MW minimum production, according to the data sets. The dataset includes data from 2015 and 2016's March at a 15-minute interval. The forecasting horizons of 15 minutes out to 180 minutes out are investigated in order to provide a full evaluation of the generalisation capabilities of these approaches. Seasonal considerations led to the data set's division into spring, summer, fall, and winter subsets. The data set is split into a training set and a testing set, one for each season. The training set is used to teach the prediction models how to make predictions, while the testing set is used to check how well the models did. Here, we use the first two months the final month for testing across all three months of data that make up each season..

4.2. Performance evaluation scheme

Models' ability to anticipate is typically assessed by contrasting their predictions with actual results. Mean absolute error (MAE), root coefficient of determination can be used to examine how well PV output power is estimated (R2). Below you'll see the criteria that will be used for ranking.:

$MAE = \frac{1}{N}\sum_{n\in N}\left|P_n^m - P_n^f\right|$ (26)

$RMSE = \sqrt{\frac{1}{N}\sum_{n\in N}(P_n^m - P_n^f)^2}$ (27)

P nm is the actual power output as measured, while P nf is the anticipated power output based on the total number of test samples, N. Predictive model accuracy improves when mean absolute error and root mean squared error (MAE and RMSE, respectively) decrease, and as R2 becomes closer to 1, indicating that the model is more efficient.

Table 1: Analysis of Proposed Model on different Season

Season	Metrics	VGGNet	DenseNet	Proposed
Spring	MAE	17.646	8.980	5.383
	RMSE	26.499	16.062	9.565
Summer	MAE	16.047	6.274	3.624

	RMSE	24.679	9.892	5.879
Fall	MAE	6.329	3.551	2.146
	RMSE	13.264	7.248	4.356
Winter	MAE	8.251	5.105	2.781
	RMSE	17.144	11.672	5.815
Average	MAE	12.069	5.529	3.484
	RMSE	20.401	11.219	6.404

When the season is spring, the proposed model achieved 9% of RMSE and 5.38% of MAE, where the DenseNet achieved 8.90% of MAE and 16.06% of RMSE and VGGNet achieved 26% of RMSE and 17.64% of MAE. From this analysis, it is clearly proves that the proposed model achieved better performance. In the analysis of RMSE, DenseNet achieved 9.89% on summer, 7.24% on fall, 11.67% on winter and 11.219% on average, where the proposed model achieved 5.87% on summer, 4.35% on fall, 5.81% on winter and 6.40% on average. Figure 1 presents the graphical investigation of projected model with existing procedures.

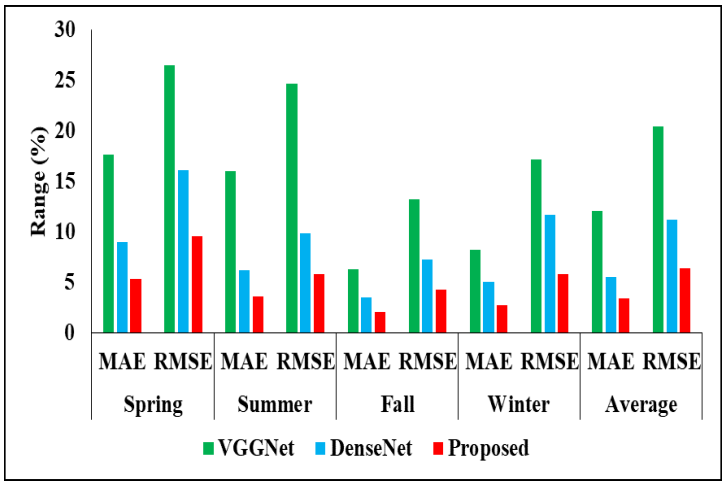

Figure 1: Graphical Comparison of Projected Model

TABLE 2. Average MAE figures in terms of numerous prediction horizons.

Methods	**30-min**	**60-min**	**90-min**	**120-min**
VGGNet	8.162	15.914	23.270	30.343
DenseNet	3.434	7.812	12.420	17.126
AlexNet-ARO	2.167	4.898	7.753	10.699

For 30-min analysis, the proposed model achieved 2.167% of MAE, VGGNet achieved 8.162% and DenseNet achieved 3.434%. The proposed model achieved 7.75% of MAE, VGGNet achieved 23.270% and DenseNet achieved 12.420% for 90-mins analysis. When the min analysis is high, the performance of all techniques is also high. For instance, the proposed model achieved 10.699% of MAE, VGGNet achieved 30.343% and DenseNet achieved 17.126% of MAE for 120-mins. Figure 2 presents the graphical analysis.

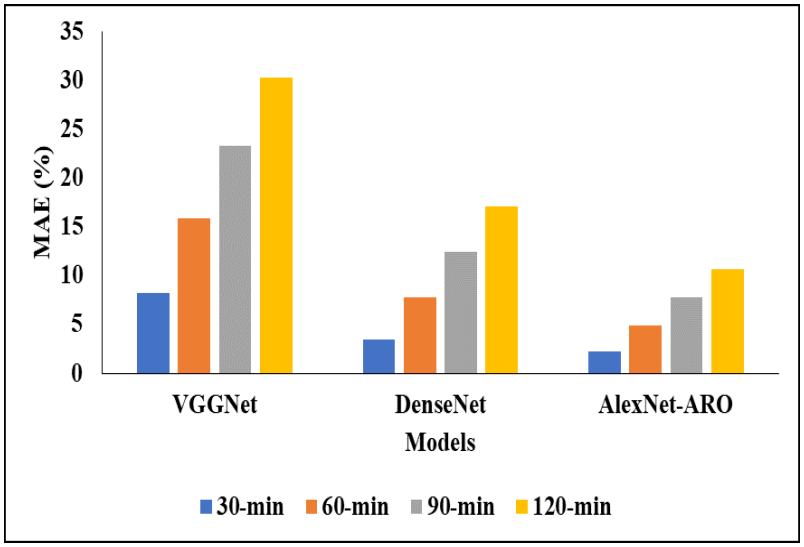

Figure 2: Comparative analysis of proposed model.

Table 3. Recognition effectiveness of baseline DL models.

Methods	**Accuracy**	**Loss**	**F-Measure**
LeNet	85.07% (±0.807%)	0.37 (±0.023)	84.58% (±1.359%)
ResNet	82.10% (±6.612%)	0.49 (±0.177)	77.84% (±16.350%)
VGGNet	82.77% (±1.851%)	0.40 (±0.018)	81.79% (±4.511%)
DenseNet	81.96% (±1.690%)	0.39 (±0.017)	81.93% (±2.228%)
AlexNet	81.57% (±1.729%)	0.41 (±0.040)	81.00% (±3.661%)
Proposed	85.78% (±2.027%)	0.35 (±0.027)	86.75% (±1.989%)

In above Table 3. Recognition effectiveness of baseline DL models. In the analysis of LeNet model reached the accuracy as 85.07% (±0.807%) and loss of 0.37 (±0.023) and F-measure as 84.58% (±1.359%) correspondingly. Then the ResNet model reached the accuracy as 82.10% (±6.612%) and loss of 0.49 (±0.177) and F-measure as 77.84% (±16.350%) correspondingly. Then the VGGNet model reached the accuracy as 82.77% (±1.851%) and loss of 0.40 (±0.018) and F-measure as 81.79% (±4.511%) correspondingly. Then the DenseNet model reached the accuracy as 81.96% (±1.690%) and loss of 0.39 (±0.017) and F-measure as 81.93% (±2.228%) correspondingly. Then the AlexNet model reached the accuracy as 81.57% (±1.729%) and loss of 0.41 (±0.040) and F-measure as 81.00% (±3.661%) correspondingly. Then the Proposed model reached the accuracy as 85.78% (±2.027%) and loss of 0.35 (±0.027) and F-measure as 86.75% (±1.989%) correspondingly.

V. CONCLUSION

A growing number of people are turning to solar power as a sustainable alternative. A difficult problem that guarantees crucial decision assistance in the design and operation of

PVPP. The short-term prediction issue in PV power generation systems is discussed, and an artificial intelligence-based solution is proposed. We set up a hybrid deep learning architecture and link together data from two consecutive days, which can prove to be quite valuable in real-world applications. These methods of prediction utilise data on solar power gathered from operational wind generators in Limberg. Compared to state-of-the-art approaches used as benchmarks, As can be seen from those aforementioned simulation results, the proposed technique results in extremely little prediction errors. While the focus of this work is on the short-term prediction problem of PV power generation, it is important to note that the and energy systems. The features are used as input to a convolutional neural network, and the retrained network is then used to make PV power predictions. A PVPP logs power usage, temperature, radiation, and wind speed over time. In addition, the ARO model is used to identify the best values for the AlexNet hyper-parameters. The collected findings demonstrate that the suggested strategy significantly outperforms the worst performing forecast method.

Data Availability Statement

The dataset used in this research work is publicly available and it is taken from the Reference [16]

REFERENCES

1. de Oliveira, R.A., Ravindran, V., Rönnberg, S.K. and Bollen, M.H., 2021. Deep learning method with manual post-processing for identification of spectral patterns of waveform distortion in PV installations. IEEE Transactions on Smart Grid, 12(6), pp.5444-5456.
2. Manno, D., Cipriani, G., Ciulla, G., Di Dio, V., Guarino, S. and Brano, V.L., 2021. Deep learning strategies for automatic fault diagnosis in photovoltaic systems by thermographic images. Energy Conversion and Management, 241, p.114315.
3. Zhang, C., Li, Z., Jiang, H., Luo, Y. and Xu, S., 2021. Deep learning method for evaluating photovoltaic potential of urban land-use: A case study of Wuhan, China. Applied Energy, 283, p.116329.
4. Sridharan, N.V. and Sugumaran, V., 2021. Visual fault detection in photovoltaic modules using decision tree algorithms with deep learning features. Energy Sources, Part A: Recovery, Utilization, and Environmental Effects, pp.1-17.
5. Zhong, T., Zhang, Z., Chen, M., Zhang, K., Zhou, Z., Zhu, R., Wang, Y., Lü, G. and Yan, J., 2021. A city-scale estimation of rooftop solar photovoltaic potential based on deep learning. Applied Energy, 298, p.117132.
6. [Qu, Y., Xu, J., Sun, Y. and Liu, D., 2021. A temporal distributed hybrid deep learning model for day-ahead distributed PV power forecasting. Applied Energy, 304, p.117704.
7. [Mellit, A. and Kalogirou, S., 2021. Artificial intelligence and internet of things to improve efficacy of diagnosis and remote sensing of solar photovoltaic systems: Challenges, recommendations and future directions. Renewable and Sustainable Energy Reviews, 143, p.110889.
8. Demirci, M.Y., Beşli, N. and Gümüşçü, A., 2021. Efficient deep feature extraction and classification for identifying defective photovoltaic module cells in Electroluminescence images. Expert Systems with Applications, 175, p.114810.
9. [Venkatesh, S.N. and Sugumaran, V., 2021. Fault Detection in aerial images of photovoltaic modules based on Deep learning. In IOP Conference Series: Materials Science and Engineering (Vol. 1012, No. 1, p. 012030). IOP Publishing.
10. [Berghout, T., Benbouzid, M., Ma, X., Djurović, S. and Mouss, L.H., 2021, October. Machine learning for photovoltaic systems condition monitoring: A review. In IECON 2021–47th Annual Conference of the IEEE Industrial Electronics Society (pp. 1-5). IEEE.

11. [Luo, X., Zhang, D. and Zhu, X., 2021. Deep learning based forecasting of photovoltaic power generation by incorporating domain knowledge. Energy, 225, p.120240.
12. [Zaki, S.A., Zhu, H., Fakih, M.A., Sayed, A.R. and Yao, J., 2021. Deep-learning–based method for faults classification of PV system. IET Renewable Power Generation, 15(1), pp.193-205.

13. W. Lee, K. Kim, J. Park, J. Kim, and Y. Kim, ‘‘Forecasting solar power using long-short term memory and convolutional neural networks,’’ IEEE Access, vol. 6, pp. 73068–73080, 2018.
14. Y.-J. He, Y.-C. Zhu, J.-C. Gu, and C.-Q. Yin, ‘‘Similar day selecting based neural network model and its application in short-term load forecasting,’’ in Proc. Int. Conf. Mach. Learn. Cybern., vol. 8, 2005, pp. 4760–4763.
15. [X. Sun, P. B. Luh, K. W. Cheung, W. Guan, L. D. Michel, S. S. Venkata, and M. T. Miller, ‘‘An efficient approach to short-term load forecasting at the distribution level,’’ IEEE Trans. Power Syst., vol. 31, no. 4, pp. 2526–2537, Jul. 2016.
16. [Elia. Belgium’s Electricity Transmission System Operator. Accessed: Jan. 13, 2020. [Online]. Available: https://www.elia.be/en/griddata/power-generation/solar-pv-power-generation-data.